Reduced Dyes Enhance Single-Molecule Localization Density for Live Superresolution Imaging

Lina Carlini,[a] Alexander Benke,[a] Luc Reymond,[b] Gražvydas Lukinavičius,[b] and Suliana Manley*[a]

Cell-permeable rhodamine dyes are reductively quenched by NaBH$_4$ into a non-fluorescent leuco-rhodamine form. Quenching is reversible, and their fluorescence is recovered when the dyes are oxidized. In living cells, oxidation occurs spontaneously, and can result in up to ten-fold higher densities of single molecule localizations, and more photons per localization as compared with unmodified dyes. These two parameters directly impact the achievable resolution, and we see a significant improvement in the quality of live-cell point-localization superresolution images taken with reduced dyes. These improvements carry over to increase the density of trajectories for single-molecule tracking experiments.

1. Introduction

Live-cell superresolution (SR) imaging based on stochastic optical reconstruction microscopy (STORM) or photoactivated localization microscopy (PALM)[1] requires cycling of dyes between fluorescent and dark states, in an environment established by the cell.[2] The cellular environment does not significantly perturb the photoswitching of fluorescent proteins, but this is not the case for synthetic dyes, which are highly sensitive to endogenous reducing and oxidizing agents. Typically, synthetic dyes in a fluorescent state are targeted to cells, and dark states are induced in situ by the generation of radical species at high laser powers.[2a, b, e, 3] Other, more controlled means of quenching dyes into a dark state by chemical modification exist, and are broadly used in bioimaging to create sensors of the cellular environment, revealing the local concentration of ions, metabolites, or other analytes.[4]

One example of controlled quenching is the case of reduced dyes, which are produced by incubation with a reducing agent. Reduced cyanine dyes have several interesting properties: their fluorescence is recovered by oxidation with superoxides or hydroxyl radicals, and their increased hydrophobicity can sometimes render them cell-permeable.[5] As such, they have found use as sensors of intracellular reactive oxygen species in tissues, cells and in vivo,[5] and as intermediates in the synthesis of photoactivatable dyes.[6] Intriguingly, several cyanine dyes directly become photoactivatable upon reduction,

and when stochastically switched into a fluorescent state by UV light they can be used as ultra-stable labels for fixed-cell STORM imaging.[7] These properties of improved control over the dye fluorescent state and enhanced single-molecule photon yields are also advantageous for live-cell SR imaging. However, although it has been proposed,[8] reduced dyes have not thus far been used in such a manner.

In this work, we use sodium borohydride (NaBH$_4$) to reduce commonly used cell-permeable rhodamine-based dyes, thereby quenching their fluorescence. We show that their fluorescence is recovered upon oxidation. Furthermore, their fluorescence recovery occurs spontaneously when they are targeted to proteins in living cells, and does not require any exogenous chemicals or light. The properties of the reoxidized dye are attractive for live-cell SR imaging, since they are more photostable and yield higher densities of single molecules.

2. Results and Discussion

2.1. Reversible Reduction of Rhodamine-Based Dyes

Reduction of 5,6-carboxyrhodamine 110 (505) or 6-carboxytetramethylrhodamine (TMR) was performed in the presence of NaBH$_4$ (see the Experimental Section). Both dyes showed rapid quenching of fluorescence, and their peak absorbance decreased by approximately 160-fold (505) and 33-fold (TMR) (Figure 1a). Oxidation by Fenton's reagent, which produces two reactive oxygen species, the hydroxyl radical and hydrogen superoxide, dramatically increased their fluorescence. Absorption spectra were measured after centrifugation to remove iron precipitates, a by-product of Fenton's reaction. After correcting for a shift in the baseline due to incomplete removal of the precipitates, we observed a significant recovery, 85% (505) and 50% (TMR), of the absorbance relative to the unmodified dyes.

[a] L. Carlini, A. Benke, Prof. S. Manley
Laboratory of Experimental Biophysics
Institute of Physics of Biological Systems
École Polytechnique Fédérale de Lausanne (EPFL)
National Centre of Competence in Research (NCCR) in Chemical Biology
Lausanne (Switzerland)
E-mail: suliana.manley@epfl.ch

[b] Dr. L. Reymond, Dr. G. Lukinavičius
Institute of Chemical Sciences and Engineering
École Polytechnique Fédérale de Lausanne (EPFL)
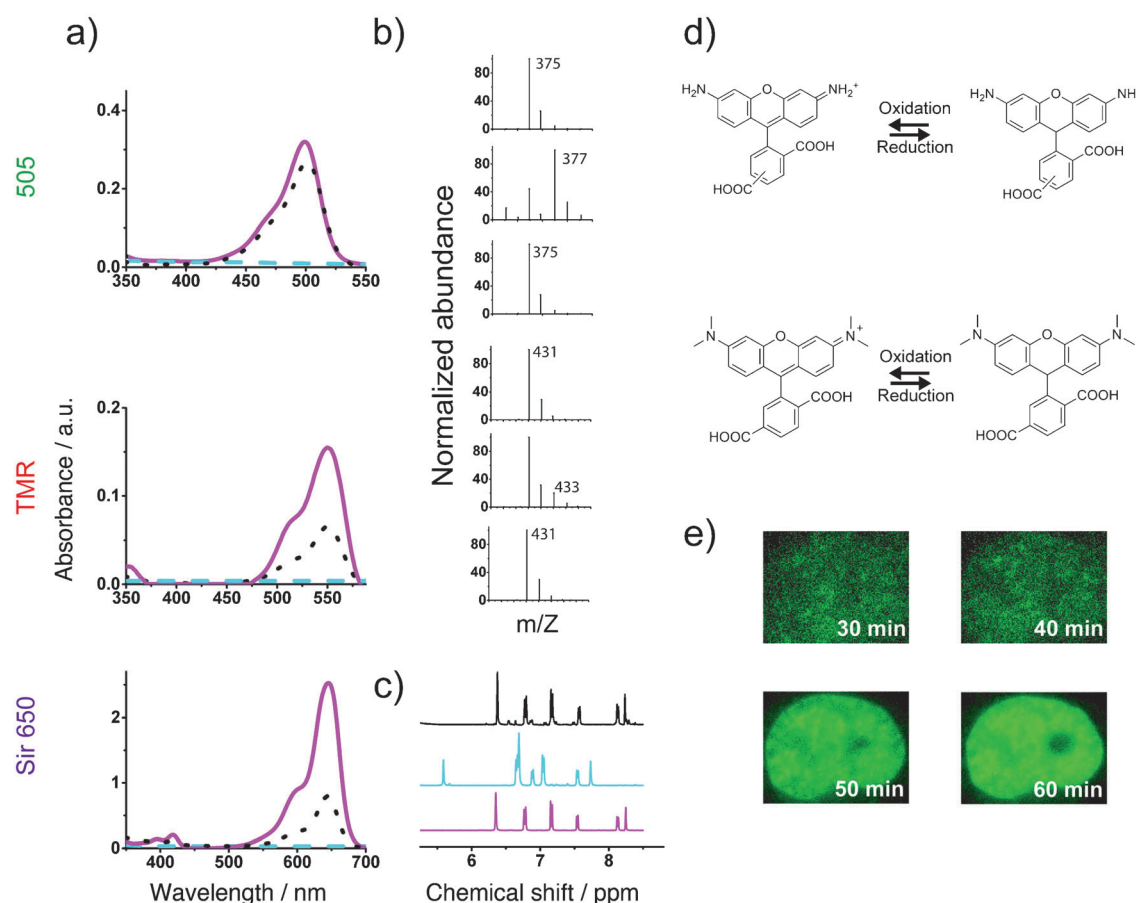National Centre of Competence in Research (NCCR) in Chemical Biology
Lausanne (Switzerland)

Figure 1. Demonstrating reversible reduction by NaBH$_4$. a) Absorbance of unmodified dye (magenta line), dye upon addition of NaBH$_4$ (cyan dashed line), and reoxidized dye once Fenton's reagent was added (black dotted line). 505, TMR, and Sir 650 in top, middle, and bottom panel, respectively. b) MS data of the unmodified dye (top), reduced dye (middle), and reoxidized dye (bottom). First set of three MS spectra for 505, second set of three MS spectra for TMR. c) NMR spectra for TMR in its unmodified (magenta), reduced (cyan), and reoxidized (black) form; ammonium persulfate was used to reoxidize TMR. d) Structure of the oxidized and reduced (leuco) forms for 505 (top) and TMR (bottom); *m/z* values for the oxidized and reduced forms of 505 are 375 and 377, respectively. For TMR, the oxidized and reduced forms correspond to 431 and 433, respectively. e) Recovery of fluorescence with BG 505 labeling H2B SNAP in the nucleus over the course of 60 min.

We performed liquid chromatography mass spectrometry (LCMS) to examine the structural basis for these changes in absorbance spectra. Reduction of rhodamines produces the known non-fluorescent leuco-rhodamine form.[9] LCMS analysis of the reaction of 505 with NaBH$_4$ confirmed the conversion of the dye (*m/z* 375 Da, retention time 2.6 min) into a new compound with a different retention time of 2.3 min, devoid of absorbance at 505 nm and with *m/z* of 377 Da (Figure 1 b, top). This observation is consistent with the formation of the leuco-form of 505 (Figure 1 d, top). The reduced sample also shows a minor peak with *m/z* 375 Da, but this is most likely an artifact from the electrospray ionization process. Reduction of rhodamines is a reversible process. Therefore, LCMS analysis of the reduced 505 sample treated with Fenton's reagent showed complete recovery with *m/z* of 375 Da, and an identical retention time to 505 before reduction with NaBH$_4$. Treatment of BG-505 with NaBH$_4$ gave similar results. We observed a new product without absorbance at 505 nm and with a 2 Da increased *m/z*. This suggests that the reduction of BG-505 with NaBH$_4$ yields BG-leuco-505 without altering the benzlyguanine part of the molecule.

We repeated LCMS measurements for TMR, and similarly found that the dye (*m/z* 431 Da, retention time 2.9 min) was converted upon reduction into a new compound with a different retention time (*m/z* 433 Da, 3.4 min), devoid of absorbance at 550 nm as shown in Figure 1 b, bottom. This new species is most likely the leuco-form of TMR (Figure 1 d, bottom). Here, the reduced sample showed a significant peak at *m/z* 431 Da, which we believe was due to the oxidation of TMR during the electrospray ionization process. Upon addition of the Fenton reagent to the reduced-TMR dye, we recover TMR (*m/z* 431 Da, retention time 2.9 min). To further validate our interpretation, we acquired nuclear magnetic resonance (NMR) spectra of TMR (Figure 1 c, magenta curve). The spectra of the reduced TMR (Figure 1 c, cyan curve) is an unambiguous proof of TMR conversion to a leuco-form. Since the iron from Fenton's reagent would have altered the NMR spectra, we used ammonium persulfate instead; upon addition of this oxidant, the reduced dye returned (Figure 1 c, black curve) to its fluorescent form.

We hypothesized that the recovery of fluorescence could also occur in an unperturbed cellular environment, as reactive

oxygen species are always present in living systems, and could substitute for the role of Fenton's reagent in the in vitro experiments. We stained cells expressing H2B-SNAP with the reduced form of BG-505. Indeed, time-lapse imaging revealed a recovery of fluorescence which we noticed continuously increased over the course of ~ 60 min (Figure 1 d). A similar recovery of fluorescence was observed for BG-TMR. Both dyes maintained their cell-permeable properties, as evidenced by their ability to stain proteins in the nucleus.

In one key difference with reduced cyanine dyes, neither of these rhodamine-based dyes displayed an increased absorption in the UV region upon reduction by NaBH4 (Figure 1 a). Interestingly, a similar effect was observed with oxazine dyes, which have the same backbone as rhodamines.[10] We therefore expected that UV illumination would not influence dye recovery. This was confirmed in live cells stained with reduced dyes, where no increase in fluorescence was observed upon exposure to 405 nm light. This is not the case for semi-reduced radical ion off states, where absorption in the UV has been observed[11] and dye recovery can be enhanced by UV illumination.

2.2. Live-Cell STORM SR Imaging with Reduced Rhodamine-Based Dyes

Given the reversibility of their fluorescence quenching, we tested the dyes in living cells to see whether their single-molecule properties were sufficient for SR imaging. The optimal dyes are stable, giving many photons before photobleaching to allow for high localization precision. They should also have a photoswitching rate that permits a high density of single molecules to resolve the structure within a short time, while preserving a minimum average distance between molecules in the "on" state so that they can be readily localized.[2d, 12]

We stained cells expressing the histone H2B protein fused to the SNAP tag (H2B-SNAP) with either the unmodified BG-505 or its reduced form. We acquired a stack of raw images for SR analysis for cells of similar fluorescence intensity. We noticed that the density of molecules in each frame appeared significantly higher for cells stained with the reduced dye. Consistent with this, cumulative localization densities from a stack of 6000 images were ninefold higher, and we saw a similar improvement for TMR when it was reduced (Table 1). The images rendered from single molecule localizations were dramatically improved for the reduced dyes (Figure 2). Indeed, the unmodified dyes, while suitable for single-molecule tracking,[13] did not
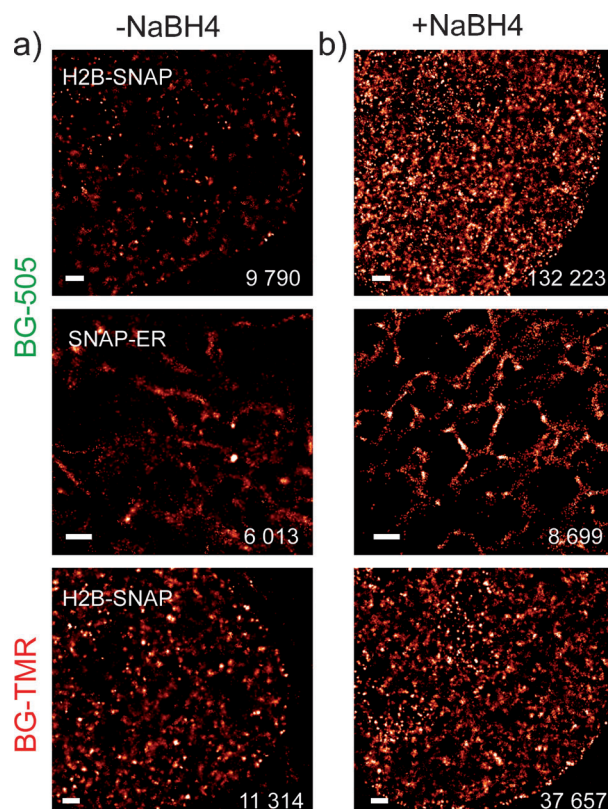

Figure 2. SR with reduced dyes at 2 kW cm^{-2}. a) Cells labeled with unmodified dye and b) reduced dyes. Number of localizations displayed, showing density enhancement for the reduced case. All data was acquired with a 30 ms exposure for 3 min. Scale bar: 1 μm.

provide high enough localization densities for SR imaging (Figure 2a).

We also tested whether a similar effect could be observed in the endoplasmic reticulum (ER). Cells expressing the ER retention sequence fused to the SNAP tag (ER-SNAP) were labeled with reduced or unmodified BG-505. Without reducing BG-505 prior to labeling the ER, molecules bleached too rapidly even at the lowest powers tested. As a result, the structure of the ER is not well sampled and the image contains spurious localizations. In contrast, labeling the ER with reduced BG-505 allowed the dye to photoswitch, yielding enough molecules to outline this organelle's meshwork of tubes.

We found improvement in dye performance upon reduction in two different organelles: the nucleus and ER. We do not expect similar oxidation kinetics in different organelles. Indeed, some compartments may not successfully reoxidize the reduced dye. Therefore, to apply this strategy to different intracellular compartments, the choice of reduced dye should be based on the local chemical environment. For instance, unmodified 505 and TMR photoswitch in the nucleus, but bleach too rapidly in the endoplasmic reticulum. As a result, SR imaging is not possible with this dye/organelle combination.

The far-red dye silicon-rhodamine-carboxyl SiR-carboxyl[14] is also rhodamine-based and cell-permeable, and we found that its fluorescence was fully quenched when reduced by NaBH$_4$. Spectroscopic data showed that its absorbance recovered upon incubation with Fenton's reagent, although to a lesser

Table 1. Quantification of dye performance. Values are the average of 2–3 cells imaged at 2 kW cm^{-2}. Errors in brackets are standard deviation values.

Dye	Molecular Density per unit time [molecules per μm^{2}s^{-1}]	Mean photons per molecule
505	0.15 (0.03)	4740 (47)
505+NaBH$_4$	1.39 (0.22)	7477 (70)
TMR	0.33 (0.08)	2320 (147)
TMR+NaBH$_4$	1.08 (0.13)	2461 (109)

extent than 505 or TMR (30%) (Figure 1 c). SiR-SNAP also recovered fluorescence when targeted in living cells. However, we found that its single-molecule densities were not improved by reduction, perhaps because of inefficient reversal of the reduction.

2.3 Live-Cell Compatibility

It can be challenging to fulfill the requirements for high-quality SR imaging while maintaining the health of living cells. This is because high laser powers are typically needed to induce dyes to photoswitch efficiently. In fixed cells, buffers containing reducing agents and an oxygen scavenging system can be freely used to optimize dye properties for SR imaging.[15] In contrast, in living cells, photoswitching rates and dye photon yields depend on the local chemical environment set by cellular processes, and any additives should not impact cell health. We wondered whether reduced dyes could be used for SR under preferred live-cell fluorescence imaging conditions. A first indication that this may be the case is the observation that we could obtain high densities of molecules (Figure 2) in Leibovitz medium, without adding any exogenous reducing or oxidizing agents. Leibovitz is a standard medium that supports the growth of cells without added CO_2. Additionally, we explored the effect of labeling cells with reduced dyes by performing the 3-(4,5-dimethylthiazol-2-yl)-2,5-diphenyltetrazolium bromide (MTT) viability assay 24 h after labeling. The results indicate that cell health is not compromised in cells labeled with the reduced dye.

We tested the effect of laser power on single-molecule density. For the reduced dye, we found that the density of molecules decreased as laser power was increased (Figure 3 a, black symbols); this effect could serve as a means to control imaging density. These differences translate into marked differences in the quality of the SR images (insets, Figure 3 a). Typically, the density of molecules is much less sensitive to the laser power, as seen for the unmodified dye (Figure 3 a, red symbols). In addition, the molecular density was always greater for the reduced dye than the unmodified dye, by a factor of 2–10 depending on the power.

The difference between the reduced and unmodified dyes is shown in more detail in Figure 3 b, where we plot the time dependence of the localization density, normalized to 1 at the peak. The unmodified dye falls off rapidly (Figure 3 a, red), while the reduced dye maintains a higher density of localizations for a longer time period (Figure 3 a, black).

2.4. Single-Molecule Tracking

Another interesting application for photoswitchable dyes is single-molecule tracking.[2c] We and others have shown that synthetic dyes targeted to intracellular compartments can be tracked at relatively high densities.[13, 16] Under even lower laser intensities than used for SR imaging (0.1 kW cm^{-2}), we collected single-molecule images and tracked their positions over time. We found that the reduced form of BG-505 gave strikingly higher densities of trajectories. In the case of the histone
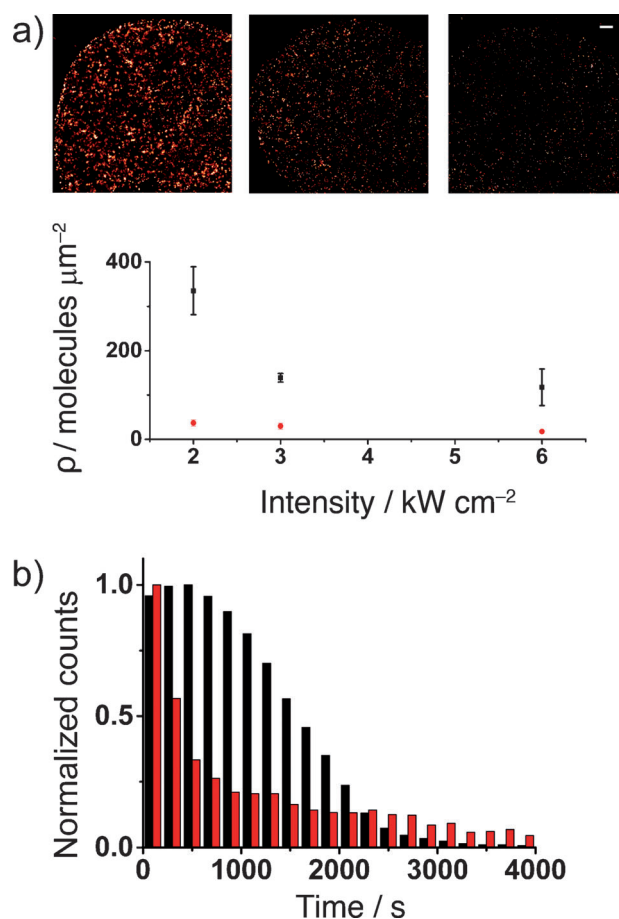

Figure 3. Density enhancement with reduced dyes. a) The molecular density, ρ, as a function of imaging intensity for the reduced (black line) and unmodified (red line) BG-505 labeling H2B-SNAP in the nucleus; values are the average of 2–3 cells per condition, error bars are standard deviation values. Density were determined over 3.5 min, 30 ms exposure time. Inset: representative SR images of reduced BG-505 labeling H2B for each laser intensity measured. Scale bar: 2 μm. b) Normalized localization counts over time for reduced (black) and unmodified (red) BG-505 labeling H2B-SNAP in the nucleus.

protein H2B, we measured more than an order of magnitude more tracks than with the unmodified dye (Figure 4a). Although track densities were very different, the distributions of track lengths were not (Figure 4b), as quantified by measuring the decay constant, which differed by ~20%. This demonstrates that the "on" times of the dyes are quite similar, so any differences in photoswitching duty cycle should be due to differences in "off" times.

3. Conclusions

We reversibly reduced cell-permeable rhodamine-based dyes by NaBH$_4$ to enhance their performance for live-cell point-localization SR. We found that dyes were more stable, and yielded higher localization densities after they had been reduced. In the previously reported case of cyanine dyes, it was found that single molecules imaged in fixed cells gave orders of magnitude more photons after reduction by NaBH$_4$ and reactivation with UV light. No mechanism has been proposed for this dra-
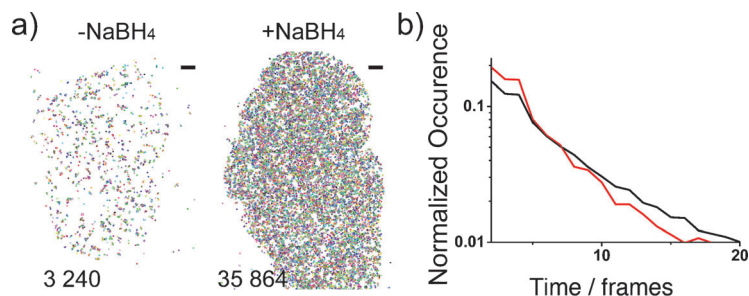
Figure 4. Single-particle tracking with reduced BG-505 at 0.1 kW cm^{-2}. a) Trajectory maps of H2B-SNAP BG-505 molecules, which were either (left) unmodified or (right) reduced. Tracks equal to or longer than five frames are plotted. Scale: 2 μm. Data was acquired with a 30 ms exposure for 3 min. b) Normalized distribution of track lengths for the reduced (red line) and unmodified (black line) BG-505 labeling H2B in the nucleus with average track lengths of 3.9 ($\pm$ 0.1) and 5.0 ($\pm$ 0.1), respectively.

matic increase in stability, which we observe in living cells to a much lesser extent.

As for the increase in the density of molecules with the reduced dye, we can conceive of two factors that may both contribute. The number of dyes in the dark state that can be converted back into a fluorescent state may be higher, or the time constants between dark and fluorescent states may be modified. We speculate that the improvement in localization density is due to differences in the nature of the dark states. In the case of the unmodified dye, molecules are transferred into a dark state by exposure to intense excitation light. This can give rise to a number of different dark states,[11,17] which do not necessarily have a pathway to become fluorescent again on the timescale of these experiments, or may be irreversibly photobleached. Here, dyes were put into a largely reversible dark state by reduction with NaBH$_4$, and were gradually returned to a fluorescent state, most likely by reoxidation with cellular reactive oxygen species. We noticed that fluorescence on a bulk level took several hours to reach a steady state. Thus, the dyes were continuously being reoxidized during our experiment. This process would provide a continuous supply of dyes to be converted back into a fluorescent state and localized for our SR images. As a result, we expect that the improvement in localization density is greatest during this recovery period. We expect the recovery time scale to vary between organelles due to differences in their oxidation potentials. We also noticed that dye "on" times, as revealed by single-molecule tracking, were nearly unchanged. This suggests that only the "off" times may have changed, becoming shorter to increase the fluorophore duty cycle.

Intriguingly, a relationship between single-molecule blinking and chromophore structure has been observed, whereby red and far-red fluorophores have longer "off"-times and more pronounced blinking, making them more suitable for SR imaging. This is the case for cyanine,[18] carbocyanine, and BODIPY dyes.[3a] It was shown that this is due differences in dye reduction potential, with redder dyes of a chromophore series having higher reduction potentials, and thus a more stable radical-ion "off" state.[18] Our observation here with the reducing agent NaBH$_4$ is that the bluest dye (505) responded well, with the highest level of fluorescence recovery, and the red-

dest dye (SiR) recovered the least, with similar trends for localization densities. This indicates that the strategy of reduction can render dyes suitable for SR imaging, increasing the choice of blue and green labels.

We confined our study to rhodamine-based dyes that were known to be cell-permeable, even in their unmodified form. However, it has been reported that reduction can also increase the cell permeability of dyes. The improved photophysical properties of reduced dyes can enhance SR image quality, and other dyes should be similarly examined.

Experimental Section

Cell Culture and Sample Preparation

U2OS cells were cultured in DMEM Glutamax-I media (Gibco/Invitrogen) in a 5% CO2 atmosphere at 37 °C supplemented with 10% FBS (Invitrogen). Cells were plated on 25 mm round size one coverslips (Mentzell), which were cleaned in pure ethanol and flamed. Approximately 24 h after plating, transient transfections with H2B-SNAP and ER-SNAP were performed (1 μgDNA + 3 μL Fugene6 - Roche). Imaging was performed 24 h after transfection; staining was performed just prior to imaging. All imaging was performed in Lebovitz medium (Gibco) at room temperature.

Dye Reduction and Sample Staining

Dye at a concentration of 1.25 μm was reduced using 10–50 mm of NaBH$_4$, which had been dissolved in PBS for 10 min. The reduced dye was then diluted five times in phenol-free DMEM or Leibovitz. Cells were stained for 30 min with the reduced BG-fluorescent substrate (NEB) (BG-505 or TMR) and washed three times in PBS. Between PBS washes, cells were incubated for 5 min in a 5% CO2 atmosphere at 37 °C with phenol-free DMEM.

Live-Cell Superresolution Imaging

Imaging was performed on an inverted microscope (IX71, Olympus), equipped with an oil-immersion objective (UPlanSAPO 100 x, NA = 1.40, Olympus). A 488 nm (Sapphire 488, Coherent) was used to excite BG-505, a 561 nm (Sapphire 561, Coherent) laser was used for TMR a 641 nm (Cube 641, Coherent) laser was used for testing Sir-650. Fluorescence was directed onto an electron-multiplying CCD camera (iXon+, Andor) with a resulting pixel size of 100 nm. Laser intensities were determined as follows: the laser powers were measured directly after the objective and the beam spot size was estimated by imaging a coverslip. A Gaussian profile was fit to the laser beam image and the FWHM was used to estimate an effective area over which the beam energy was dispersed. Laser intensities were between 0.1–6 kW cm^{-2}. In order to minimize drift, the sample holder was bolted into place on a motorized stage driven by a piezo (PINANO, PhysikInstrument). For each dye, typically 7000 to 15000 frames were collected with a 30 ms exposure time per frame; 2–5 cells were imaged for each laser intensity tested. Molecules were localized using the Peakselector software (courtesy of Herald Hess) where detected peaks were fit to a 2D Gaussian using a non-linear least squares fitting algorithm. Peaks with a width between 80–300 nm in both x and y directions and having 200–2000 photons were considered to be good single mol-

ecule localizations. Unless otherwise noted, peaks with a localization precision better than 50 nm were selected for analysis.

Data Analysis

Raw data was analyzed using Peakselector software provided by Harald Hess. Peaks were selected based on their parameters: peak width, number of photons, and localization precision. Peaks with a width between 80 nm and 250 nm, 200–2000 photons, and localization precision less than 50 nm were considered as good single-molecule localizations. A standard grouping procedure was also applied to group molecules appearing in consecutive frames. dSTORM images were rendered as a sum of superimposed filtered peaks with a width corresponding to their empirically determined localization precision.

Single-Particle Tracking

Single-particle tracking was performed using a script written in Matlab (The Mathworks, Inc., Natick, MA). Briefly, localizations were assigned to the same molecule if they were closer than a given radius (100 nm) and the gap between them was equal or less than two frames.

Absorbance Measurements

Absorbance spectra were collected on a UV-1800 Shimadzu UV spectrophotometer. Dyes were measured at concentrations between 3–5 µm. For absorbance measurements of reduced dyes, 50 mm of $NaBH_4$ was incubated with the dye for 10 min. Reduced dye was reoxidized using Fenton's reagent (40 mm $Fe2+$, 2 mm H_2O_2) and measured after 30 min of centrifugation at 1° to remove the iron precipitates formed from Fenton's reaction. Identical solutions were measured with LCMS.

LCMS

LCMS was performed on a Shimadzu MS2020 connected to a Nexerra UHPLC system equipped with a Waters ACQUITY UPLC BEH C18 1.7 µm 2.1×50 mm column. Buffer A: 0.05% HCOOH in H_2O. Buffer B: 0.05% HCOOH in acetonitrile. Analytical gradient was from 0% to 50% B within 5 min at a flow rate of 0.5 mL min^{-1}.

NMR

1.9 mg TMR was dissolved in deuterated PBS (0.8 mL) and a ^{1}H NMR spectrum of the dark purple solution was recorded at r.t. on a Brucker AvanceIII-400 equipped with a CPPBBO$_Z$ cryoprobe. Solid $NaBH_4$ (4.5 mg) was added to the TMR solution which was incubated at r.t. for 30 min, resulting in a colorless to light pink solution. The pH was adjusted to 3 with 2 m HCl and the reduced TMR was extracted with 1 mL ethyl acetate. The organic layer was separated and evaporated. The light pink residue was dissolved in deuterated PBS (0.5 mL) and an ^{1}H NMR spectrum of the light pink solution was recorded at r.t. Then 5 mg ammonium persulfate were added directly in the NMR tube, the pH was adjusted to 7.4 with solid $NaHCO_3$ and the solution was incubated 15 min at r.t. ^{1}H NMR spectrum of the dark purple solution was finally recorded at r.t.

Acknowledgements

[1] a) E. Betzig, G. H. Patterson, R. Sougrat, O. W. Lindwasser, S. Olenych, J. S. Bonifacino, M. W. Davidson, J. Lippincott-Schwartz, H. F. Hess, *Science* **2006**, *313*, 1642–1645; b) S. T. Hess, T. P. K. Girirajan, M. D. Mason, *Biophys. J.* **2006**, *91*, 4258–4272; c) M. J. Rust, M. Bates, X. Zhuang, *Nat. Methods* **2006**, *3*, 793–795.

[2] a) S. A. Jones, S. H. Shim, J. He, X. Zhuang, *Nat. Methods* **2011**, *8*, 499–505; b) T. Klein, A. Löschberger, S. Proppert, S. Wolter, S. Van De Linde, M. Sauer, *Nat. Methods* **2011**, *8*, 7–9; c) S. Manley, J. M. Gillette, G. H. Patterson, H. Shroff, H. F. Hess, E. Betzig, J. Lippincott-Schwartz, *Nat. Methods* **2008**, *5*, 155–157; d) H. Shroff, C. G. Galbraith, J. A. Galbraith, E. Betzig, *Nat. Methods* **2008**, *5*, 417–423; e) R. Wombacher, M. Heidbreder, S. Van De Linde, M. P. Sheetz, M. Heilemann, V. W. Cornish, M. Sauer, *Nat. Methods* **2010**, *7*, 717–719.

[3] a) L. Carlini, S. Manley, *ACS Chem. Biol.* **2013**; b) S. H. Shim, C. Xia, G. Zhong, H. P. Babcock, J. C. Vaughan, B. Huang, X. Wang, C. Xu, G. Q. Bi, X. Zhuang, *Proc. Natl. Acad. Sci. USA* **2012**, *109*, 13978–13983.

[4] a) A. Minta, J. P. Y. Kao, R. Y. Tsien, *J. Biol. Chem.* **1989**, *264*, 8171–8178; b) T. Mosmann, *J. Immunol. Methods* **1983**, *65*, 55–63; c) O. Myhre, J. M. Andersen, H. Aarnes, F. Fonnum, *Biochem. Pharmacol.* **2003**, *65*, 1575–1582; d) O. Tour, S. R. Adams, R. A. Kerr, R. M. Meijer, T. J. Sejnowski, R. W. Tsien, R. Y. Tsien, *Nat. Chem. Biol.* **2007**, *3*, 423–431.

[5] K. Kundu, S. F. Knight, N. Willett, S. Lee, W. R. Taylor, N. Murthy, *Angew. Chem.* **2009**, *121*, 305–309; *Angew. Chem. Int. Ed.* **2009**, *48*, 299–303.

[6] L. M. Wysocki, J. B. Grimm, A. N. Tkachuk, T. A. Brown, E. Betzig, L. D. Lavis, *Angew. Chem.* **2011**, *123*, 11402–11405; *Angew. Chem. Int. Ed.* **2011**, *50*, 11206–11209.

[7] J. C. Vaughan, S. Jia, X. W. Zhuang, *Nat. Methods* **2012**, *9*, 1181–1135.

[8] J. Vogelsang, C. Steinhauer, C. Forthmann, I. H. Stein, B. Person-Skegro, T. Cordes, P. Tinnefeld, *ChemPhysChem* **2010**, *11*, 2475–2490.

[9] K. Kundu, S. F. Knight, S. Lee, W. R. Taylor, N. Murthy, *Angew. Chem.* **2010**, *122*, 6270–6274; *Angew. Chem. Int. Ed.* **2010**, *49*, 6134–6138.

[10] T. Kottke, S. van de Linde, M. Sauer, S. Kakorin, M. Heilemann, *J. Phys. Chem. Lett.* **2010**, *1*, 3156–3159.

[11] S. van de Linde, I. Krstic, T. Prisner, S. Doose, M. Heilemann, M. Sauer, *Photochem. Photobiol. Sci.* **2011**, *10*, 499–506.

[12] G. T. Dempsey, J. C. Vaughan, K. H. Chen, M. Bates, X. Zhuang, *Nat. Methods* **2011**, *8*, 1027–1040.

[13] A. Benke, N. Olivier, J. Gunzenhäuser, S. Manley, *Nano Lett.* **2012**, *12*, 2619–2624.

[14] G. Lukinavičius, K. Umezawa, N. Olivier, A. Honigmann, G. Yang, T. Plass, V. Mueller, L. Reymond, I. R. Corrêa Jr, Z. G. Luo, C. Schultz, E. A. Lemke, P. Heppenstall, C. Eggeling, S. Manley, K. Johnsson, *Nat. Chem.* **2013**, *5*, 132–139.

[15] a) N. Olivier, D. Keller, P. Gönczy, S. Manley, *PLoS ONE* **2013**, *8*, e69004; b) J. C. Vaughan, G. T. Dempsey, E. Sun, X. Zhuang, *J. Am. Chem. Soc.* **2013**, *135*, 1197–1200.

[16] T. Appelhans, C. P. Richter, V. Wilkens, S. T. Hess, J. Piehler, K. B. Busch, *Nano Lett.* **2012**, *12*, 610–616.

[17] a) S. van de Linde, R. Kasper, M. Heilemann, M. Sauer, *Appl. Phys. B* **2008**, *93*, 725–731; b) J. Vogelsang, T. Cordes, C. Forthmann, C. Steinhauer, P. Tinnefeld, *Proc. Natl. Acad. Sci. USA* **2009**, *106*, 8107–8112; c) C. Steinhauer, C. Forthmann, J. Vogelsang, P. Tinnefeld, *J. Am. Chem. Soc.* **2008**, *130*, 16840–16841.

[18] I. H. Stein, S. Capone, J. H. Smit, F. Baumann, T. Cordes, P. Tinnefeld, *ChemPhysChem* **2012**, *13*, 931–937.